Controlled Evolution of Highly Elongated Tokamak Plasmas

F. B. Marcus, S. C. Jardin,[a] and F. Hofmann

Centre de Recherches en Physique des Plasmas, Association Euratom–Confédération Suisse, Ecole Polytechnique Fédérale de Lausanne, 1007 Lausanne, Switzerland

(Received 12 August 1985)

It is demonstrated numerically that a tokamak plasma can be evolved continuously from a near-circular cross-section shape to a 4/1 vertically elongated racetrack. All intermediate stages and the final state are stable to axisymmetric MHD modes. The stabilization is provided by the vacuum vessel walls on the ideal time scale and by an orthogonal active feedback system on the resistive time scale.

PACS numbers: 52.30.Jb, 52.55.Fa

We demonstrate here the feasibility of constructing a tokamak experiment to explore β_T limits in high-current, high-elongation plasmas. A limit on β_T (ratio of plasma to toroidal-field pressure) in tokamaks, scaling as I_p/aB_T, has previously been proposed and verified[1,2] in ideal-MHD calculations, for plasmas with moderate elongations up to $\kappa = 1.6$. Here I_p is the plasma current, a is the horizontal minor radius, and B_T is the toroidal field. At a fixed limiter safety factor q_Ψ, I_p increases with increasing κ at fixed a and B_T, which experimentally has allowed an increase in β_T in quasi steady-state discharges.[3] Highly elongated belt pinches[4–7] ($\kappa \sim 10$) have obtained high β_T (tens of percent), but are transient (tens to hundreds of microseconds). Ideal- and resistive-MHD studies[8] of an infinite one-dimensional plasma have indicated that high-elongation configurations may have high β_T limits. In this Letter, two key areas are specifically addressed: (1) It is demonstrated that controlled formation and maintenance of highly elongated tokamak plasmas in a realistic geometry is possible; (2) the ideal- and resistive-MHD axisymmetric stability of these plasmas is verified.

The geometry utilized in these studies is shown in Fig. 1. A rectangular vacuum vessel is placed inside two vertical stacks of field-shaping coils which form a periodic structure vertically. Limiter points are indicated with a cross. The plasma evolution proceeds as follows: A nearly circular plasma with $q_\Psi = 2$ is formed near the top of the vessel, with $R_0 = 0.80$ m, $a = 0.18$ m, $B_T = 1.5$ T, and $T_{e0} = 10^3$ eV. The MHD equilibrium and resistive simulations are begun at this point. The plasma current is then increased at the same time as the vertical elongation is increased, to 4/1 on the 10^{-1}-s time scale. The currents are programmed so as to maintain $q_\Psi \approx 2$, in order to keep the current profile as broad as possible.

The ideal-MHD equilibrium code TCVMHD[9] is used to calculate the preprogrammed coil currents for input to the time-dependent STARTUP[10] code. TCVMHD computes axisymmetric, free-boundary tokamak equilibria with a predetermined plasma shape and the coil currents necessary to produce that shape. In order to generate input data for the STARTUP code, we computed several racetrack equilibria for Table I with elongations ranging from $\kappa = 1.6$ to 4. It was found that, for fixed $q_\Psi = 2$ at the limiter, the plasma current scales with elongation approximately as

$$I_p \approx (1+\kappa^2)/2.$$

In the control system modeled in the STARTUP code, active stabilization and control is provided by four independent feedback systems for radial field (RF), quadrupole field (QF), octopole field (OF), and vertical field (VF). These systems feed back on sums and differences of the flux measurements on the flux loops

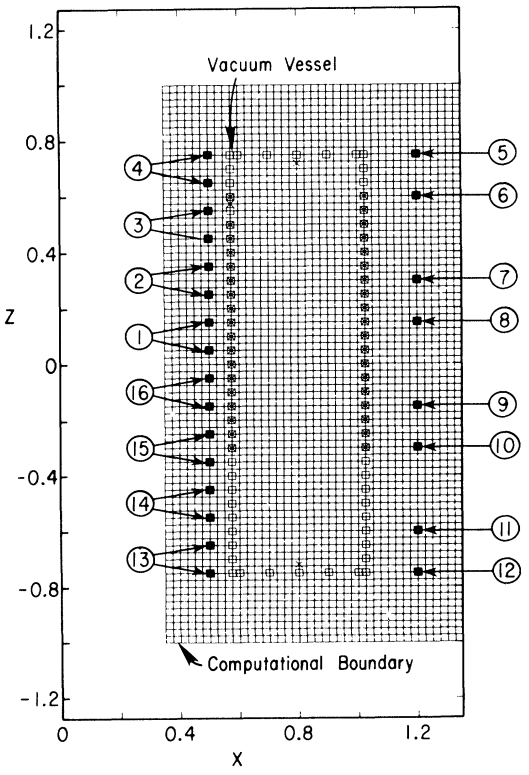

FIG. 1. Computational grid, coil, vessel, and flux-loop geometry.

© 1985 The American Physical Society

TABLE I. Preprogrammed currents (in kiloamperes) in each of the sixteen electric-field coils, plasma current, and elongation at eight reference times. Linear interpolation is used to define currents at intermediate times.

	t_1	t_2	t_3	t_4	t_5	t_6	t_7	t_8
I_1	162	164	39	-86	-110	-134	-133	-104
I_2	0	-112	-78	-80	-106	-127	-119	-96
I_3	-40	-66	-53	-58	-60	-71	-68	-48
I_4	174	218	232	224	228	199	220	240
I_5	123	91	79	71	96	99	96	105
I_6	-148	-107	-88	-93	-101	-94	-103	-108
I_7	-140	-254	-198	-153	-151	-167	-168	-154
I_8	88	80	-41	-173	-207	-174	-198	-203
I_9	0	0	-9	-4	-166	-251	-234	-203
I_{10}	0	0	65	74	90	72	-58	-154
I_{11}	0	0	0	0	0	0	-61	-108
I_{12}	0	0	0	0	0	0	132	105
I_{13}	0	0	0	0	0	0	133	240
I_{14}	0	0	0	0	0	0	-28	-48
I_{15}	0	0	131	54	176	72	-39	-96
I_{16}	0	0	49	140	-78	-131	-127.4	-104
I_p	332	541	584	763	1069	1174	1425	1700
κ	1.6	2.0	2.25	2.5	3.0	3.25	3.62	4.0

1–7 described in Table II.

A given flux measurement is in general an interpolated signal from two stationary flux loops. Thus, for example, if $t_1 < t < t_2$, then flux measurement number 1 would correspond to

$$\Psi_1(t) = \alpha\Psi(0.62, 0.43, t) + (1-\alpha)\Psi(0.62, 0.36, t), \quad (1)$$

where $\alpha = (t_2 - t)/(t_2 - t_1)$ and $\Psi(R,Z,t)$ is the poloidal magnetic flux at position (R,Z) at time t.

The state vector for the flux-loop measurements is denoted by

$$\Psi(t) = (\Psi_1(t), \Psi_2(t), \Psi_3(t), \ldots, \Psi_7(t)). \quad (2)$$

The orthogonal vectors corresponding to the four control systems are

$$\begin{aligned} \Psi_{RF} &= (0, +1, +1, 0, -1, -1, 0), \\ \Psi_{VF} &= (-1, -1, +1, +1, +1, -1, 0), \\ \Psi_{QF} &= (-2, +1, +1, -2, +1, +1, 0), \\ \Psi_{OF} &= (-1, -1, -1, -1, -1, -1, 6). \end{aligned} \quad (3)$$

Corresponding to each of the orthogonal flux-measurement vectors of Eq. (2) is a vector of current amplitudes $I(t)$,

$$I(t) = (I_1(t), I_2(t), I_3(t), I_4(t), I_5(t), I_6(t), I_7(t)). \quad (4)$$

TABLE II. Z position of control-flux loops used at eight reference times. At intermediate times, the control flux is interpolated with use of the loop positions in the table. Flux loops 1, 2, and 6 have $R = 0.62$ m; flux loops 3, 4, and 5 have $R = 0.98$ m; while flux loop 7 has $R = 0.8$ m, $Z = 0.72$ m.

Loop #	t_1	t_2	t_3	t_4	t_5	t_6	t_7	t_8
2 and 3	0.513	0.440	0.480	0.500	0.550	0.560	0.560	0.560
1 and 4	0.430	0.360	0.315	0.250	0.180	0.135	0.070	0.000
5 and 6	0.353	0.280	0.150	0.000	-0.190	-0.290	-0.420	-0.560

The current vectors for each of the control systems are determined by selection of coils or groups of coils near the control-flux loops at each of the eight reference times. The inductance matrix $M(t)$ between these coil groups and the control-flux loops is inverted to obtain the control-current vectors at each of the eight times,

$$\begin{aligned} I_{RF}(t) &= M_{RF}^{-1}(t)\Psi_{RF}(t), \\ I_{VF}(t) &= M_{VF}^{-1}(t)\Psi_{VF}(t), \\ I_{QF}(t) &= M_{QF}^{-1}(t)\Psi_{QF}(t), \\ I_{OF}(t) &= M_{OF}^{-1}(t)\Psi_{OF}(t). \end{aligned} \quad (5)$$

Control-current vectors at intermediate times are again defined by linear interpolation. For the plasma-current control, a "perfect" Ohmically heated system is modeled in which the poloidal flux everywhere on the computational boundary is increased at the same rate.

In the absence of plasma or additional conductors, the control systems described above are independent in the sense that the flux vector from one current vector is orthogonal to the other flux vectors. This orthogonality property is approximately preserved in the presence of conductors and plasma because of the symmetrical placement of the coils and flux loops. Thus the feedback-control voltage for each of the feedback current groups is chosen proportional to the inner product of its flux vector and the flux state vector. For example, the voltage driving the flux radial field currents is

$$V_{RF}(t) = \gamma\Psi_{RF}\Psi(t), \quad (6)$$

where γ is a proportionality constant.

The STARTUP code[10] is a free-boundary axisymmetric simulation code which models the resistive-time-scale evolution of a toroidal plasma, including its interaction with the poloidal-field coils and other nearby conductors. Circuit equations for the poloidal-field systems are solved simultaneously with the plasma equations, allowing realistic modeling of passive and active feedback systems. The plasma is modeled as a

distributed-current resistive fluid whose shape and size change dynamically during the evolution to remain in near MHD equilibrium, with a single point of contact with the limiter or magnetic divertor. Flux-surface-averaged transport equations evolve the two-fluid adiabatic variables and the rotational transform, together with the entropy and number density for each species. The computation is carried out numerically on a background Eulerian grid on which grid points may be one of three types: conductor, vacuum, or plasma. The vacuum is modeled as a cold (here 2.5 eV) pressureless plasma. The plasma flux surfaces, including the moving plasma-vacuum interface, are continuously contoured to compute the surface-averaged metric quantities.

The disparate time scales in the equations are handled numerically by artificial enhancement of the ion mass and viscosity to slow down and damp Alfvén waves, and by the substepping of the flux-diffusion and fast Alfvén terms. The Alvén velocity has been reduced by a factor of $\mu = 4500$ in the runs reported here, and a normalized viscosity coefficient of $\nu = 8.0$ was used. We have verified that these artificially large parameters do not affect the motion of the plasma on the L/R time scale of the passive coils when realistic values of resistivity and inductance are used.

The vacuum vessel is modeled as a discrete set of 72 conductors spaced 0.05 m apart. The time constant of each conductor is 12 ms, corresponding to a vacuum vessel of thickness 0.025 m with a resistivity of 10^{-7} Ω m. Independent induced currents develop in each of the 72 conductors; however, a constraint is imposed such that the sum of the 72 currents always equals zero, modeling a gap. The time constant for response of the feedback systems is also 12 ms.

If the plasma becomes ideal-MHD unstable during its evolution, this instability will grow on the modified Alfvén time scale, which is an order of magnitude faster than the resistive decay time of the conductors or the time scale over which the preprogrammed or feedback currents are changing. This instability motion is thus readily distinguished from the stable resistive evolution. As a check, we rerun a stable evolution sequence twice, once with the Alfvén velocity-reduction factor μ set equal to 3000 and once with the artificial viscosity parameter $\nu = 12.0$. These should give results that are indistinguishable from the original run, verifying that plasma inertia is unimportant, and thus ideal-MHD instabilities are absent.

The computation is initialized to the equilibrium configuration shown in Fig. 2(a). The plasma is shown to evolve in a stable manner through the states shown in Figs. 2(b) through 2(d). Examination of the current required in the feedback systems shows that a maximum feedback current of 20 kA was required to maintain positional control of the plasma during the evolution. The plasma was thus evolved up to the maximum 4/1 elongation at $\beta_T = 2.3\%$, with axisymmetric stability found at all times. Initial studies indicate that β_T up to the Troyon limit[1] has little effect on the axisymmetric stability.

We plot the Z position of the plasma centroid versus time as curve A in Fig. 3. Curves B and C show the result for the same calculation repeated with the mass-enhancement parameter $\mu = 3000$ and with the artificial viscosity $\nu = 12$. The near identity of these three curves verifies the axisymmetric stability during the calculation. For comparison, we plot additional curves D, E, and F in Fig. 3 corresponding to reruns of the original calculation with the feedback systems turned off and the vacuum vessel walls removed at times t_1, t_3, and t_6 (Table I). In these cases, axisym-

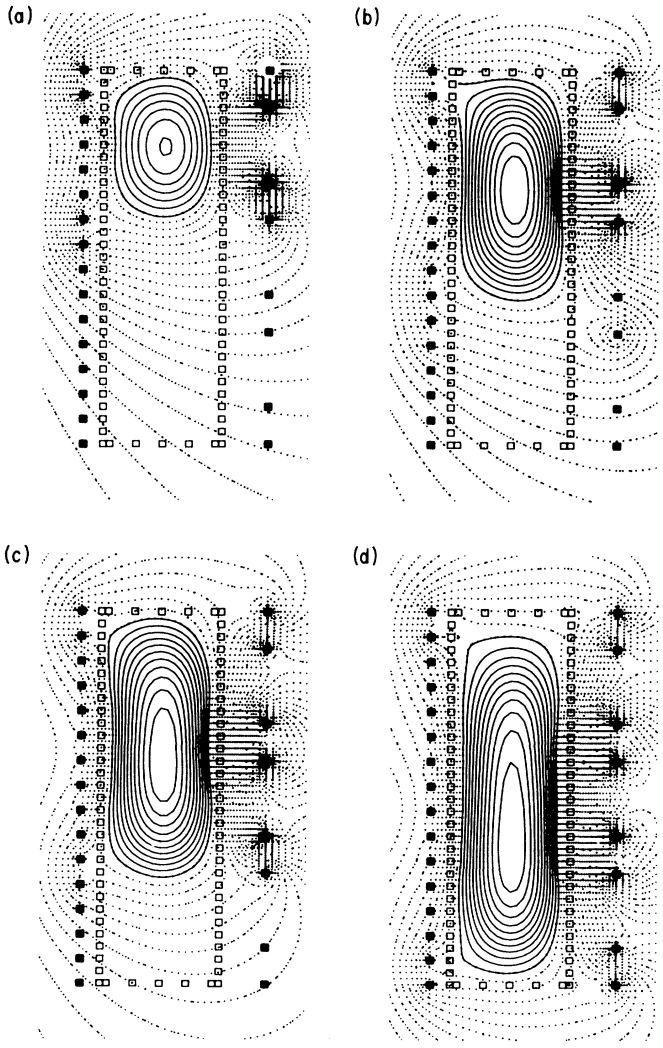

FIG. 2. Flux-surface geometry for a stable evolution sequence at (a) $t = t_1 = 0$, (b) $t = t_3 = 0.075$ s, (c) $t = t_5 = 0.137$ s, and (d) $t = t_8 = 0.210$ s.

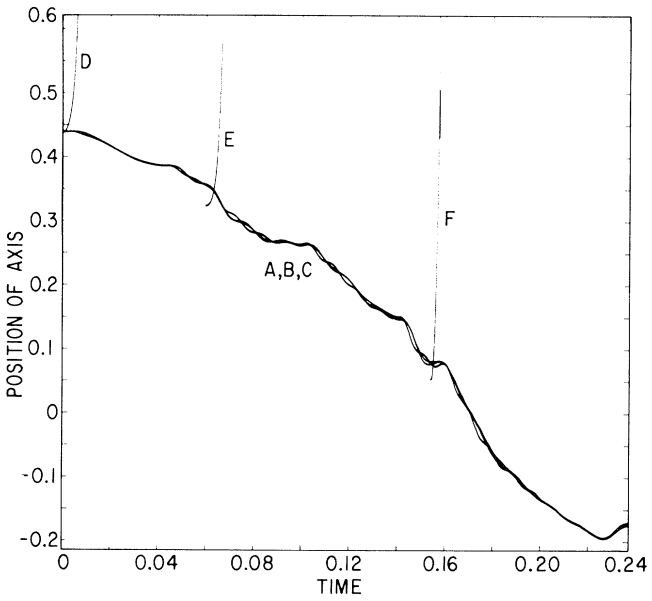

FIG. 3. Simulation results of Z position of magnetic axis vs time for a physical sequence with mass enhancement and viscosity parameters as follows: Curve A, $\mu = 4500$, $\nu = 8.0$; curve B, $\mu = 3000$, $\nu = 8.0$; and curve C, $\mu = 4500$, $\nu = 12.0$. Curves D, E, and F illustrate ideal-MHD instability when the passive conducting walls are removed.

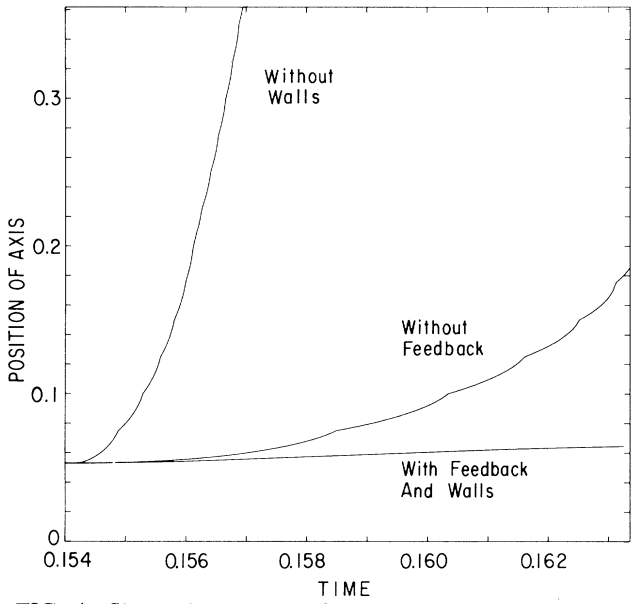

FIG. 4. Simulation results of Z position of magnetic axis vs time for different conditions illustrating the time scales of stable formation, resistive instability, and ideal instability.

metric instability on the ideal time scale is evident.

To demonstrate the separation of time scales in the simulation, we plot in Fig. 4 simulation results for $0.154\ \text{s} < t < 0.163\ \text{s}$ of the Z position of the magnetic axis versus time for the standard case (feedback and walls), an ideal-MHD–unstable case with the conducting walls removed at $t = 0.154$ s, and a resistive-unstable case with the active feedback system shut off at $t = 0.154$ s. The disparate time scales are evident.

In conclusion, we have found and simulated a method for obtaining highly elongated tokamak plasmas on the 10^{-1}-s time scale by using a combination of preprogrammed currents, passive conductors, and an orthogonal feedback system. The equilibria all have $q_\Psi \approx 2$ at the limiter and broad, but not hollow, current profiles consistent with the MHD evolution equations assuming classical Spitzer resistivity. The continuously evolved equilibria between a near-circular plasma and a 4/1 elongated racetrack plasma are all stable to both ideal and resistive axisymmetric MHD modes.

We wish to thank Professor F. Troyon, Dr. R. Gruber, Dr. N. Pomphrey, and Dr. J. DeLucia for useful discussions and comments. This work was partly supported by the Swiss National Science Foundation and by the U.S. Department of Energy through Contract No. DE-AC02-76-CH0-3073.

[a]On leave from Plasma Physics Laboratory, Princeton University, Princeton, N.J. 08544.

[1]F. Troyon, R. Gruber, H. Saurenmann, S. Semenzato, and S. Succi, Plasma Phys. Controlled Fusion **26**, 209 (1984).

[2]A. Sykes, M. F. Turner, and S. Patel, in *Proceedings of the Eleventh European Conference on Controlled Fusion and Plasma Physics, Aachen, 1983* (European Physical Society, Petit-Lancy, Switzerland, 1983), Vol. 2, p. 363.

[3]K. H. Burrell *et al.*, Nucl. Fusion **23**, 536 (1983).

[4]K. H. Dippel *et al.*, in *Proceedings of the Fifth International Conference on Plasma Physics and Controlled Nuclear Fusion, Tokyo, 1974* (International Atomic Energy Agency, Vienna, 1975), Vol. 3, p. 57.

[5]F. Hofmann, Nucl. Fusion **15**, 336 (1975).

[6]C. K. Shu *et al.*, in *Proceedings of the Sixth International Conference on Plasma Physics and Controlled Fusion, Bertschesgaden, 1976* (International Atomic Energy Agency, Vienna, 1977), Vol. 1, p. 511.

[7]G. Becker *et al.*, in *Proceedings of the Seventh International Conference on Plasma Physics and Controlled Fusion, Innsbruck, 1978* (International Atomic Energy Agency, Vienna, 1979), Vol. 2, p. 115.

[8]M. S. Chance, H. P. Furth, A. H. Glasser, and H. Selberg, Nucl. Fusion **22**, 187 (1982).

[9]F. Hofmann and F. B. Marcus, Ecole Polytechnique Fédérale de Lausanne Report No. LRP 235/84, 1984 (unpublished).

[10]S. C. Jardin, in *Computational Techniques,* edited by B. Cohen and J. Brackbill (Academic, New York, 1985); S. C. Jardin, N. Pomphrey, and J. DeLucia, to be published.